

# Nano-Scale Simulation for Advanced Gate Dielectrics

● Chioko Kaneta   ● Takahiro Yamasaki   ● Yuko Kosaka

*(Manuscript received January 14, 2003)*

As a result of aggressive scaling of CMOS (Complementary Metal-Oxide-Semiconductor) transistors, the thickness of the gate insulator is approaching atomic dimensions. In advanced CMOS with such ultrathin dielectric films, atomic-scale phenomena play an important role in performance and reliability. Simulation is a powerful tool for investigating and understanding atomic scale phenomena. We investigated the electronic properties of the Si(100)/SiO<sub>2</sub> interface with the first-principles molecular dynamics method. The behavior and the electronic properties of the defect, hydrogen, and nitrogen atoms at the interface, which have a serious influence on the electronic properties of the insulating film, were also investigated. We also simulated the annealing behavior of aluminates and silicates of Hf and Zr, which are candidates for the high-dielectric-constant gate dielectric materials of future CMOS, by employing the classical molecular dynamics method. From the results of our simulation, we can obtain a guideline to control the gate dielectric materials and the interfaces with the Si substrate.

## 1. Introduction

The existence of SiO<sub>2</sub> has been one of the keys in the success of the Si-based semiconductor industry. The thin SiO<sub>2</sub> layer with the quality required for the gate insulator can be formed by thermal oxidation of the Si substrate. It has been used as the gate insulator for more than three decades.

As a result of aggressive scaling of CMOS (Complementary Metal-Oxide-Semiconductor) transistors, the thickness of the SiO<sub>2</sub> gate insulator is 2 nm or less, which is approaching the atomic dimension. (There are only about seven SiO<sub>2</sub> molecular layers in a 2 nm-thick insulating film.)

Much work continues to be done to decrease the physical and electrical thicknesses of the SiO<sub>2</sub>-based layers toward the physical limits while maintaining high quality.

On the other hand, high-k insulating metal oxides are currently being considered as future

gate-dielectric materials to replace SiO<sub>2</sub> gate dielectrics. High-k insulating metal oxides permit the use of physically thicker gate dielectrics to obtain the same effective capacitance as thinner SiO<sub>2</sub> gate dielectrics while significantly preventing direct tunneling. The thickness of the high-k insulating film is, however, also a few nm.

Thus, an understanding of atomic-level phenomena is required to control the properties of the gate insulators and to fabricate MOS devices with high performance and reliability.

Simulation is a powerful tool for investigating and understanding atomic-scale phenomena and complementing experiments. At present, progress in the art of simulation and computer technology enables us to deal with nano-scale systems not only with classical molecular dynamics but also with quantum mechanical methods.

This paper presents the results of two kinds of

nano-scale simulations for advanced gate dielectrics.

In Section 2, the electronic properties of the Si(100)/SiO<sub>2</sub> interface and the defects and impurities introduced there are investigated by employing the first-principles molecular dynamics method, which is one of the quantum mechanical calculations.

In Section 3, the crystallization of (HfO<sub>2</sub>)<sub>1-x</sub>(SiO<sub>2</sub>)<sub>x</sub>, (HfO<sub>2</sub>)<sub>1-x</sub>(AlO<sub>1.5</sub>)<sub>x</sub>, (ZrO<sub>2</sub>)<sub>1-x</sub>(SiO<sub>2</sub>)<sub>x</sub>, and (ZrO<sub>2</sub>)<sub>1-x</sub>(AlO<sub>1.5</sub>)<sub>x</sub> at annealing is discussed on the basis of the results of classical molecular dynamics simulation. The composition dependency of the crystallization and phase separation are also described.

## 2. Quantum mechanical calculations on the electronic properties of the Si/SiO<sub>2</sub> interface

Since the advent of silicon-based electronic devices, the control of the Si/SiO<sub>2</sub> interface has been one of the key issues in the fabrication of MOS devices with high performance and reliability. At the same time, with the scaling of CMOS transistors, the ratio of the interface region to the SiO<sub>2</sub> thickness is increasing and the control of the electronic properties of the Si/SiO<sub>2</sub> interface, interface traps, and the various impurities introduced into the interface have become crucial. Direct observations of the interface, however, are often difficult because it is a “buried surface.”

We investigated the electronic properties of the Si(100)/SiO<sub>2</sub> interface with first-principles molecular dynamics. In this paper, we discuss the variation of the band gap, the defect states due to the Si dangling-bonds at the Si(100)/SiO<sub>2</sub> interface, the reaction path for the dissociation of the H atom terminating the Si dangling-bond, and the behavior of the N atom at the interface.

### 2.1 Calculation method

The electronic properties of the Si(100)/SiO<sub>2</sub> interface were carried out by employing first-principles molecular dynamics<sup>1)</sup> based on the density functional theory.<sup>2)</sup> We used a norm-conserving

pseudopotential for Si atoms and ultrasoft pseudopotentials<sup>3)</sup> for O, H, and N atoms, respectively. The generalized gradient correction<sup>4)</sup> was taken into account for the exchange-correlation potential. The spin polarization was also taken into account to calculate the interface states.

The unit cell for the Si(100)/SiO<sub>2</sub> interface without defects and impurities contains seven Si layers, SiO<sub>2</sub> layers, H atoms terminating the dangling bonds at the surfaces of SiO<sub>2</sub> and Si, and a vacuum layer. There are 35 to 106 atoms in the unit cell. In the optimization process, two bottom Si layers and the H atoms at the Si surface are fixed. We investigated defects and H and/or N atoms at the interface by introducing them to the stable structure of the Si(100)/SiO<sub>2</sub> interface mentioned above and optimizing their configurations.

### 2.2 Models of the abrupt Si(100)/SiO<sub>2</sub> interface without defects and impurities

Many experiments have been carried out on the Si(100)/SiO<sub>2</sub> interface structure, and several models that suggest the existence of crystal phases of SiO<sub>2</sub> have been proposed.<sup>5)-7)</sup> The density of the SiO<sub>2</sub> in the interface region has also been measured.<sup>8)</sup> In spite of the investigations, however, the basic structural model of the Si(100)/SiO<sub>2</sub> interface is not well established.

We investigated the stability of three model structures of the abrupt Si(100)/SiO<sub>2</sub> interface with no dangling-bonds and impurities by first-principles molecular dynamics.<sup>9),10)</sup>

We prepared two kinds of SiO<sub>2</sub> layers about 1.5 and 0.7 nm thick for each SiO<sub>2</sub> structure on a seven-layer Si substrate. The thicker (about 1.5 nm) layer consists of a 4.5, 4.5, or 5 SiO<sub>2</sub> molecular layer of, respectively, quartz, tridymite, or pseudo β-cristobalite (deformed β-cristobalite so as to match the lattice spacing to that of the Si substrate). The thinner (about 0.7 nm) layer consists of 2 SiO<sub>2</sub> molecular layers of each type.

Comparing the calculated total energies obtained after the structural optimization, we found

that the interface that consists of tridymite-type  $\text{SiO}_2$  on Si (type-T) is the most stable structure when the layer is thin (about 0.7 nm). For the thicker layer (about 1.5 nm), however, the type-T becomes less stable because of the compressive stress in the  $\text{SiO}_2$ , and the optimized quartz-type  $\text{SiO}_2$  (type-Q) becomes the most stable one. The change of stability of the  $\text{SiO}_2$  layer will cause a structural change in the whole layer or in the region away from the interface during the oxide growth.

### 2.3 Electronic property of Si(100)/ $\text{SiO}_2$ interface

At the Si(100)/ $\text{SiO}_2$  interface, the electronic property changes from a semiconductor-like property to an insulator-like one. It is very important to know the change in atomic scale ultrathin gate insulators. Variation of the band gap perpendicular to the interface was calculated for the thicker layers with the above-mentioned optimized model structures.<sup>9,10</sup> The result for the type-Q is shown in **Figure 1**. In the  $\text{SiO}_2$  region from the structural interface to a point about 0.1 nm away from it, which contains the first oxygen layer, the band gap remains as narrow as that of silicon. The drastic change of the band gap takes place in the  $\text{SiO}_2$  region between about 0.1 and 0.4 nm. These are the new aspects obtained from our calculation. In the other two types of  $\text{SiO}_2$  layers, the band gap changes similarly to that of the type-Q, although the barrier heights slightly depend on the  $\text{SiO}_2$  structures. An experimental result corresponding to our calculation has been obtained by Muller et al.<sup>11</sup> The difference between the position of the structural interface and that defined by the change of the band gap will give different models of the interface, depending on the method of observation.

### 2.4 Silicon dangling bonds at the Si(100)/ $\text{SiO}_2$ interface as an origin of interface states

Interface states or traps are exceedingly harmful to the performance and reliability of MOS devices. The Si dangling-bond (SDB) defects, which

are the typical intrinsic defects at the Si/SiO<sub>2</sub> interface, have been considered to be one of the origins of the interface states or traps. They have been called  $P_b$  centers, which is a generic name for different SDB defects. It is known that the  $P_{b0}$  and  $P_{b1}$  centers in the Si(100)/SiO<sub>2</sub> interface are SDB-type defects.<sup>12-14</sup> (The  $P_{b0}$ -type defect is also found at the Si(100)/Si<sub>3</sub>N<sub>4</sub> interface.<sup>15</sup>) A high correlation between the interface state density obtained by the capacitance voltage (CV) measurement and the level density of  $P_{b0}$  and  $P_{b1}$  centers by electron paramagnetic resonance (EPR) measurement has been shown on (100) wafers.<sup>14</sup>

The  $P_{b0}$  is modeled as a  $\bullet\text{Si}=\text{Si}_3$  defect. (The symbol  $\bullet$  represents an unpaired Si bond.) The  $P_{b1}$  had been tentatively assigned to  $\bullet\text{Si}=\text{Si}_2\text{O}$ , but recent findings suggest that it exists on a Si-Si dimer and contains no O atoms.<sup>16</sup> Understanding the electronic properties of various types of SDB defects is important for Si/SiO<sub>2</sub> interface engineering.

We investigated the interface states due to the two prototypes of SDB defects at the Si(100)/SiO<sub>2</sub>.<sup>17</sup>

As a model of the Si(100)/SiO<sub>2</sub> interface with no SDBs, we employed the type-T structure.<sup>9,10</sup> A prototype of SDB defect  $\bullet\text{Si}=\text{Si}_3$  was introduced

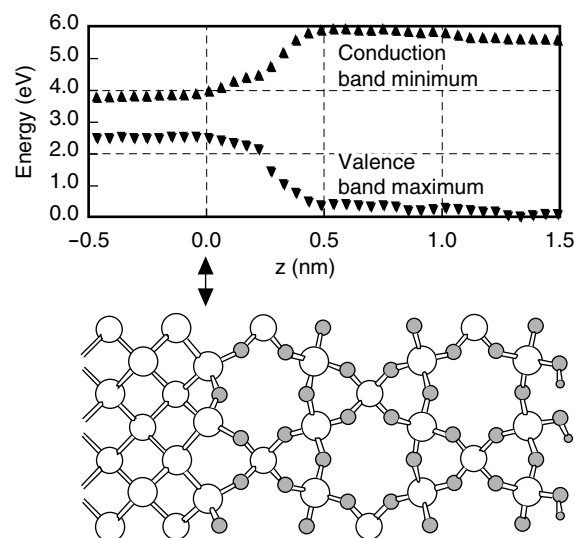


Figure 1 Energy band gap variation in the type-Q structure perpendicular to the interface. The origin of the coordinate  $z$  is taken at the interface.

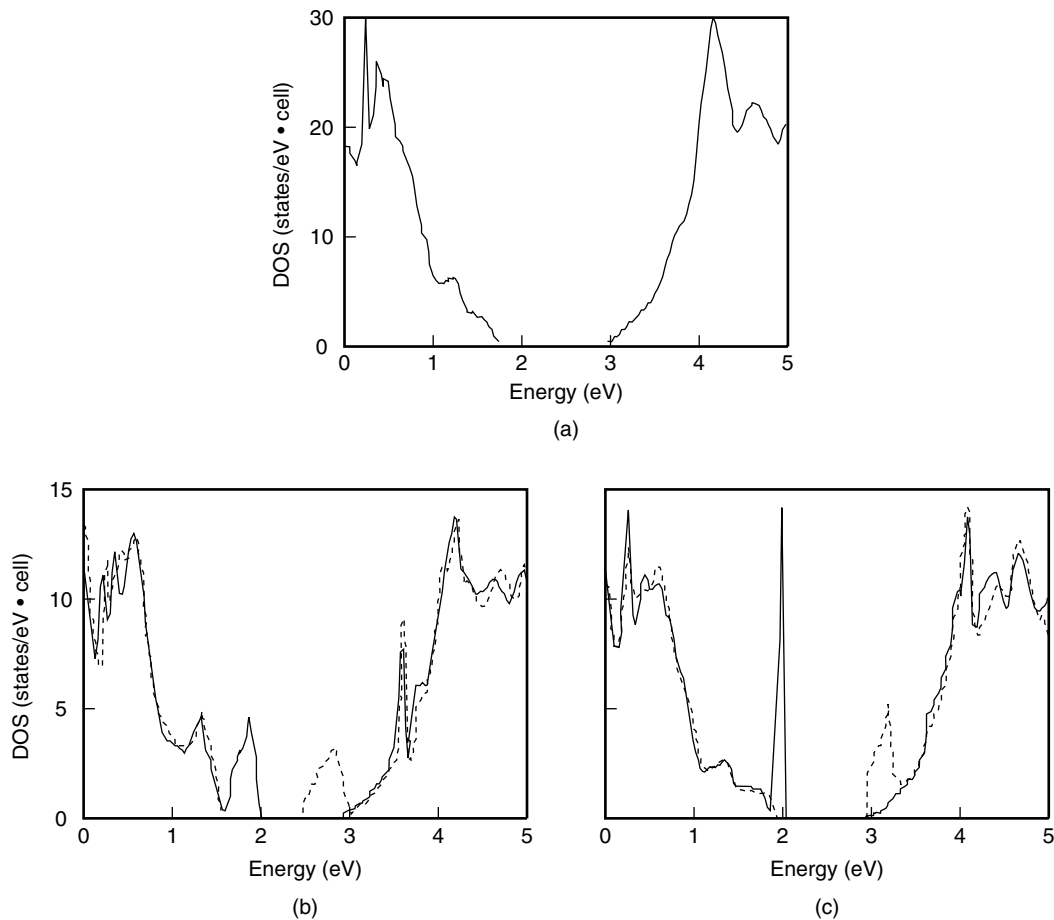


Figure 2  
Densities of states for the interface containing (a) no SDB, (b) SDB0, (c) SDB1. In (b) and (c), the densities of states for up and down spin states are shown separately with solid and dotted lines, respectively. In (a), total densities of states are shown with solid lines.

into the interface. We call this defect SDB0. This includes a  $\bullet$ Si-Si dimer and no O atom, which is basically the same structure as a recently proposed model for the  $P_{b1}$  center.<sup>16),18)</sup> To examine the structural dependence, we also modeled a system including another type of SDB defect  $\bullet$ Si $\equiv$ Si<sub>2</sub>O, which includes a  $\bullet$ Si-O bond instead of a  $\bullet$ Si-Si dimer and is labeled as SDB1.

The electron densities of states (DOSs) for the optimized atomic configurations of SDB0 and SDB1 systems were calculated to investigate the interface states that are due to them. The results are shown in **Figure 2**. For SDB0, two defect states appear in the band gap. The lower state is occupied, and the upper one is unoccupied in the neutral charge state. This corresponds to the results of

the CV and EPR measurements.<sup>14)</sup> By examining the contribution of these states to the charge density distribution, we found that the states are strongly localized on the SDB0 at the interface. The SDB1 also generates two defect states around the gap. But in this case, both of the states exist near the band edges. The interpretation of this result is somewhat delicate. But, from the comparison with the result of the Si(100)/SiO<sub>2</sub> system with no SDB at the interface shown in Figure 2 (a), we consider that the lower level is in the band gap and the upper level is in the conduction band. This does not correspond to the CV and EPR measurements on the  $P_{b0}$  and  $P_{b1}$  centers. However, the interface states located at 7 and 17 meV above the conduction band of Si have been observed by tun-

neling current spectroscopy.<sup>19)</sup>

The interface states are completely eliminated by terminating the SDBs with H atoms.

## 2.5 Dissociation of hydrogen atoms at the Si(100)/SiO<sub>2</sub> interface

In order to minimize the effect of the electrically active states due to the SDB-type defects, the defects are exposed to hydrogen, the idea being that the H atoms will passivate these defects by forming Si-H bonds. Dissociation of the Si-H bonds is considered to be dominant for the degradation of the interface. Controlling the passivation and depassivation of the SDB-type defects by H atoms is crucial in the fabrication of high-quality Si/SiO<sub>2</sub> interfaces. However, the dissociation mechanism of the Si-H bond at the Si/SiO<sub>2</sub> interface has been discussed only by using an analogy of the behavior of the H atom in the Si crystal or at the Si surface.<sup>20)-22)</sup>

Various positions of the H atom near the Si(100)/SiO<sub>2</sub> interface are shown in **Figure 3**. In the configuration with the H-Si≡Si<sub>3</sub> (H is in site **A**), which we label SDB0-H, we found no defect states in the calculated electron DOS of the band gap region of Si.

On the basis of the results of our calculation,<sup>23)</sup> we compared the difference of the total energy between both sides of the reaction SDB0-H → SDB0 + H for various configurations of the H atom shown in Figure 3. We will now discuss the dissociation mechanism of H atoms.

We found that more than 3 eV is required to remove the H atom from the Si-H bond to an interstitial position in SiO<sub>2</sub> (site **B**). The adiabatic potential is shown in **Figure 4**. No clear energy barrier is found in the adiabatic potential for the Si-H distance. The energy needed to remove the H atom from the SDB1-H is 0.3 eV higher than that needed to remove it from the SDB0-H. The adiabatic potential for the SDB1-H → SDB1 + H also has no energy barrier.

When the H atom is removed to the bond-center (BC) site of a Si-Si in the bulk Si

(site **D**), the increase of the total energy is 2.2 eV. Site **D** is a metastable position for the H atom. The corresponding energy is 2.5 eV for the system with SDB1.

No stable or metastable positions for the H atom were found near the BC site between the defect Si (•Si) and the Si atom in the Si substrate (site **E**) for the SDB0 system. On the other hand, a metastable position of 1.6 eV was found near site **E** in the system with SDB1.

The analysis of the experimental data on the H desorption from the Si(111)/SiO<sub>2</sub> interface showed that the activation energy of the Si-H dissociation is 2.56 eV.<sup>24)</sup> The calculated energies to remove the H atom from the Si-H bond to an interstitial position in SiO<sub>2</sub> seems to be rather high, even if we consider the difference of the directions of the interfaces. The activation energy of 2.56 eV may

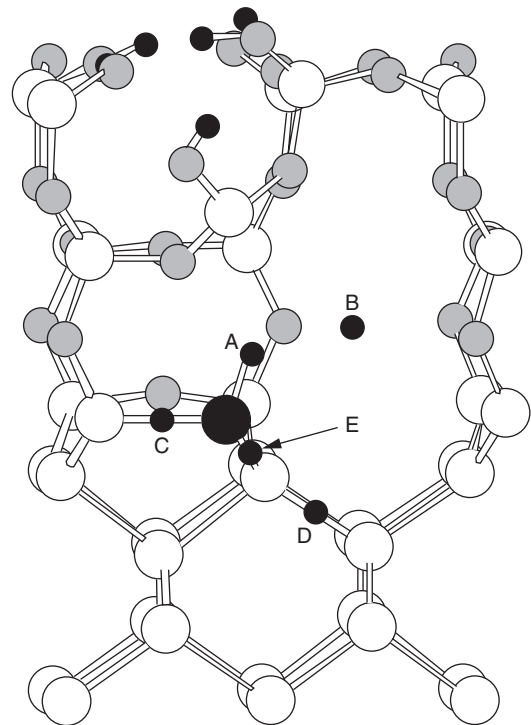


Figure 3  
Various positions of the H atom near the Si(100)/SiO<sub>2</sub> interface. Large white circles are Si atoms. The large black one is a defect Si atom. Intermediate gray and small black circles are O and H atoms, respectively. The positions in the Si-H bond (**A**), the interstitial site in SiO<sub>2</sub> (**B**), and two kinds of BC sites at the interface (**C**) and in the Si (**E**) are shown.

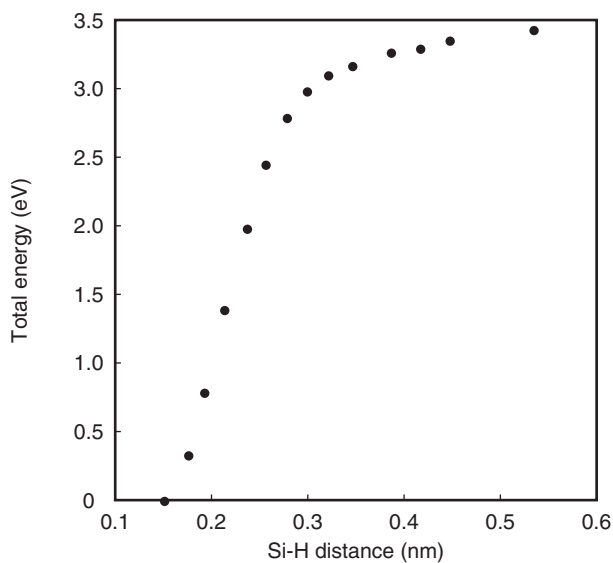


Figure 4  
Adiabatic potential for the Si-H distance in SDB0 + H (in site **A**) → SDB0 + H (in SiO<sub>2</sub>).

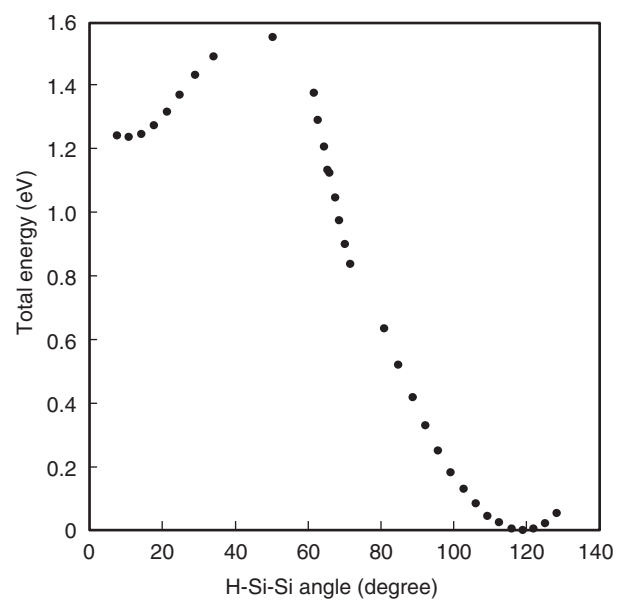


Figure 5  
Adiabatic potential for the H-Si-Si angle in SDB0 + H (in site **A**) → SDB0 + H (in site **C**).

be consistent with the H dissociation into the Si substrate. Further investigations are necessary to interpret the experimental result correctly.

The position between the two dimered Si atoms at the Si(100)/SiO<sub>2</sub> interface (site **C**) is also a metastable one for the H atom. To move the H atom to site **C** from site **A**, the required energy is 1.2 eV, which is much smaller than in the above-mentioned two cases. The adiabatic potential for the H-Si-Si angle (the angle between the SDB0-H bond and the Si-Si dimer) is shown in **Figure 5**. The energy barrier of this reaction is 1.5 eV, and that of the reverse reaction is only 0.3 eV on the potential surface. Thus, the reverse reaction can easily occur to form the Si-H configuration again.

The total energies for various configurations of the H atom in the SDB0 system are compared in **Figure 6**.

In the configuration with the H atom at site **C**, new gap states are generated near the band edge of the Si. The doubly occupied state near the valence band edge is related to the defect Si, while the unoccupied state near the conduction band edge is related to the Si-H-Si structure. These levels can capture carriers. The

carrier-enhanced dissociation is one of the possible mechanisms for generating an atomic H.

## 2.6 Nitrogen segregation at the SiO<sub>2</sub>/Si(100) interface and the trap generation

In the fabrication processes of MOS devices with very thin gate insulators of SiO<sub>2</sub>, N atoms are introduced into the SiO<sub>2</sub> region to improve device characteristics by using various nitridation processes, for example, thermal annealing in NO or N<sub>2</sub>O gas ambients and remote plasma nitridation. By thermal nitridation, N atoms are incorporated in the region near the SiO<sub>2</sub>/Si interface and are coordinated to three or two Si atoms.<sup>25)</sup> Control of concentration, position, and bonding of N atoms is very crucial, because an amount of incorporated N atoms that is sufficient to prevent penetration of B atoms from the p<sup>+</sup>-gate may degrade the reliability of devices due to negative bias temperature instability (NBTI). Several researchers ascribed the acceleration of NBTI by nitridation to some reaction between N atoms and water-related materials in the SiO<sub>2</sub> layer near the

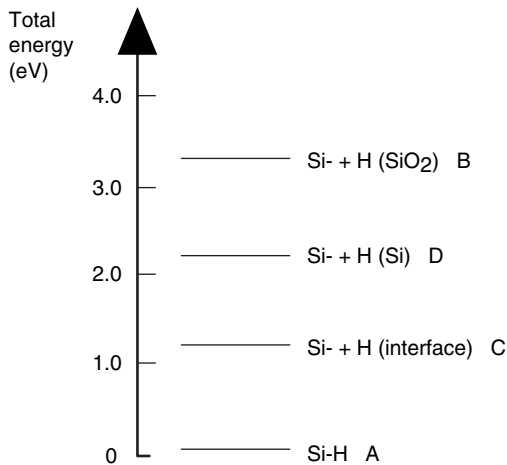


Figure 6 Comparison of the total energies for various configurations of the H atom in the SDB0 system.

interface.<sup>26)</sup> However, we have not yet reached a consensus on the mechanism. The bonding characteristics of N atoms in the SiO<sub>2</sub> region should be clarified to understand the mechanisms of N incorporation under nitridation and the mechanisms of reliability degradation.

We investigated the stabilities and electronic states of a variety of three- and two-coordinated-N-configurations near the SiO<sub>2</sub>/Si(100) interface to understand the mechanism of the N atom segregation at the interface and of hole trapping generation.<sup>27)</sup>

Two kinds of abrupt and perfect SiO<sub>2</sub>/Si(100) interface structures, that is, the type-T and Q models,<sup>9),10)</sup> are used to form Si<sub>2</sub>=N• and Si<sub>2</sub>H≡N configurations by substituting an N atom or an H-terminated N atom for an O atom in the models. Other matrices are an interface with SDB0 or SDB1.<sup>17)</sup> We substituted an N atom for a Si atom of these matrices to form three-coordinated-N-configurations: Si<sub>3</sub>≡N, Si<sub>2</sub>O≡N, and O<sub>3</sub>≡N.

We have optimized four kinds of Si<sub>2</sub>=N• and their H-terminated configurations. We label the Si<sub>2</sub>=N• configurations as shown in **Figure 7**. The Si<sub>2</sub>=N• at the interface ((T|Q)-a) is the most stable, and Si<sub>2</sub>=N• becomes less stable as it goes far

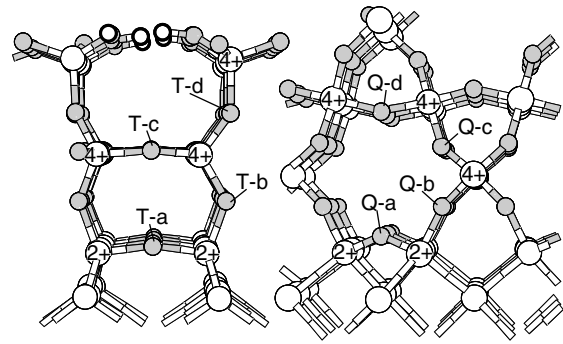


Figure 7 Labels of the O sites which are substituted by an N atom to form Si<sub>2</sub>=N• configurations, in the type-T (left-hand side) and in type-Q (right-hand side) interface structures. “2+” and “4+” on Si atoms denote anion numbers which coordinate to the Si.

Table 1 Energies of Si<sub>2</sub>H≡N configurations relative to the total energies of (T|Q)-a configurations, and Si-N-Si bond angles before and after H termination.

Site	A	B	Energy	Site	A	B	Energy
T-a	179	152	0.00	Q-a	151	137	0.00
T-b	126	127	-0.74	Q-b	159	150	+0.23
T-c	153	142	-0.42	Q-c	151	143	+0.11
T-d	137	136	-0.50	Q-d	156	147	-0.14

A: Bond angle of Si-N-Si before the H termination  
 B: Bond angle of Si-N-Si after the H termination  
 (Angle unit: degree, Energy unit: eV)

from the interface as shown in **Table 1**. These Si<sub>2</sub>=N• configurations are classified by the bonding Si atoms as ((T|Q)-a) Si<sup>2+</sup>-N-Si<sup>2+</sup>, ((T|Q)-b) Si<sup>2+</sup>-N-Si<sup>4+</sup>, and ((T|Q)-c and (T|Q)-d) Si<sup>4+</sup>-N-Si<sup>4+</sup>, where the superscript numbers correspond to the numbers of anions bonded to the Si atoms. According to these results, it is suggested that a Si<sub>2</sub>=N• around the interface has a tendency to move into the interface by thermal annealing. A Si<sup>1+</sup>-N-Si<sup>2+</sup> coordination that can be generated by insertion of an N atom into a Si-Si bond in the substrate near the interface is not stable because of accumulated stress to the bonding Si atoms. However, it could be stabilized if the stress were released enough. Si<sub>2</sub>=N• configurations have gap states which trap holes. Terminating the dangling bond with an H

atom can eliminate the gap state. Contrary to the  $\text{Si}_2=\text{N}\bullet$  stability,  $\text{Si}_2\text{H}\equiv\text{N}$  stability does not relate to the distance from the interface, but relates to the Si-N-Si bond angles of the  $\text{Si}_2=\text{N}\bullet$  before H termination in the type-T structure (Table 1). The  $\text{Si}_2\text{H}\equiv\text{N}$  configuration of (T-a) which has an open Si-N-Si bond angle before H termination is the most unstable among the four  $\text{Si}_2\text{H}\equiv\text{N}$  configurations. This kind of H-N bond would have a smaller dissociation energy compared to others.  $\text{Si}_2\text{H}\equiv\text{N}$  stability in the type-Q structure does not show such a relation with the bond angles, because Si-N-Si bond angles of  $\text{Si}_2\text{H}\equiv\text{N}$  in the type-Q are not distributed as widely as those in the type-T.

Next, we compared the  $\text{Si}_3\equiv\text{N}$ ,  $\text{Si}_2\text{O}\equiv\text{N}$ , and  $\text{O}_3\equiv\text{N}$  configurations shown in **Figure 8**. The  $\text{O}_3\equiv\text{N}$  configuration (d) is very unstable compared to the others, for example, it differs by 7.7 eV to configuration (a). The  $\text{Si}_3\equiv\text{N}$  configurations are more stable compared to  $\text{Si}_2\text{O}\equiv\text{N}$  (a') by 0.6 to 2.4 eV. Among the three  $\text{Si}_3\equiv\text{N}$  configurations, the interface  $\text{Si}_3\equiv\text{N}$  (a) is the most stable, followed in order by the second layer  $\text{Si}_3\equiv\text{N}$  (b) and the third layer  $\text{Si}_3\equiv\text{N}$  (c). The interface  $\text{Si}_3\equiv\text{N}$  (a) has no gap states. Configurations (b), (c), and (a') have gap states that can trap holes. In configurations (b) and (c), gap states due to the generated dangling bonds are located at the Si atoms near the substituted N atom. These gap states in configurations (b) and (c) can be eliminated by terminating the dangling bonds with an H atom.

When incorporated N atoms come near the interface through the  $\text{SiO}_2$  layer, they would prefer energetically to form a  $\text{Si}_2=\text{N}\bullet$  configuration at the interface. By annealing, these N would be more stabilized by substituting for SDB0s if they are close or may be stabilized by reconfiguring the surrounding networks to form a  $\text{Si}_3\equiv\text{N}$ . The other  $\text{Si}_2=\text{N}\bullet$  configurations would be stabilized by terminating their dangling bonds with H atoms. However, some  $\text{Si}_2=\text{N-H}$  configurations may have weaker N-H bonding energies due to the large Si-N-Si bond angles. These H atoms may be dissociated with relatively smaller amounts of

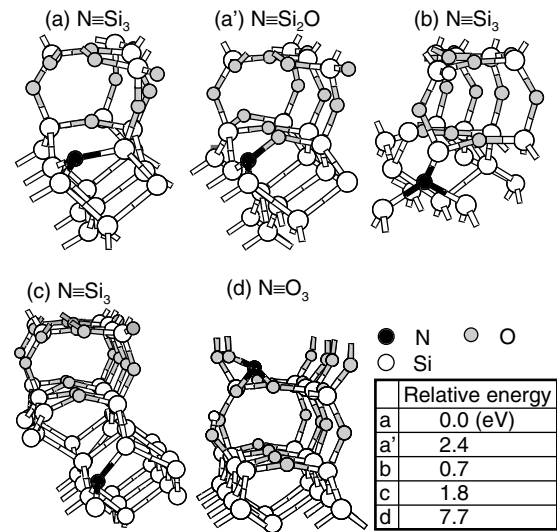


Figure 8 Three-coordinated-N-configurations. (a)  $\text{Si}_3\equiv\text{N}$  at the interface where N is substituted with SDB0, (a')  $\text{Si}_2\text{O}\equiv\text{N}$  at the interface where N is substituted for SDB1, (b)  $\text{Si}_3\equiv\text{N}$  at the second layer in the substrate, (c)  $\text{Si}_3\equiv\text{N}$  at the third layer in the substrate, and (d)  $\text{O}_3\equiv\text{N}$  in the  $\text{SiO}_2$  region.

electric stresses and/or temperature and will leave  $\text{Si}_2=\text{N}\bullet$ , which generates the hole trapping states.

### 3. Classical molecular dynamic simulation of annealing behavior of high-k gate dielectric materials

$\text{HfO}_2$  and  $\text{ZrO}_2$  are promising candidates for alternative high-k gate dielectric materials. However, they often become inhomogeneous because of the crystallization by annealing at 600 to 1000°C after deposition on the silicon substrate.<sup>28),29)</sup> In some cases, the crystallization is observed in as-deposited layers.<sup>29)</sup> The structures of the crystallized regions are reported to be monoclinic and tetragonal,<sup>29)</sup> or tetragonal or cubic.<sup>28)</sup> On the other hand,  $\text{SiO}_2$  and  $\text{Al}_2\text{O}_3$  are thermally stable, although their dielectric constants are not sufficiently high. One of the ideas for obtaining thermally stable gate dielectrics with moderately high dielectric constants is to employ alloys of ( $\text{HfO}_2$  and/or  $\text{ZrO}_2$ ) and ( $\text{SiO}_2$  and/or  $\text{Al}_2\text{O}_3$ ) as gate dielectrics. With these materials, there is a

trade-off between thermal stability and the dielectric constant. It is important to know the relation between the composition and properties under annealing in order to obtain thermally stable gate dielectric materials while keeping the dielectric constant as high as possible.

### 3.1 Model and calculation method

We investigated the composition dependency of annealing behavior and crystallization in  $(\text{HfO}_2)_{1-x}(\text{SiO}_2)_x$ ,  $(\text{HfO}_2)_{1-x}(\text{AlO}_{1.5})_x$ ,  $(\text{ZrO}_2)_{1-x}(\text{SiO}_2)_x$ , and  $(\text{ZrO}_2)_{1-x}(\text{AlO}_{1.5})_x$  for  $x$  equals 0 to 0.3 by employing the classical molecular dynamic method.<sup>30)</sup> We prepared unit cells  $3.4 \text{ nm} \times 3.4 \text{ nm} \times 5.1 \text{ nm}$  containing about 4000 atoms. To simulate the crystallization after the nucleus generation, we introduced a crystal layer of monoclinic  $\text{HfO}_2$  or  $\text{ZrO}_2$  in each cell. Amorphous  $(\text{HfO}_2)_{1-x}(\text{SiO}_2)_x$ ,  $(\text{HfO}_2)_{1-x}(\text{AlO}_{1.5})_x$ ,  $(\text{ZrO}_2)_{1-x}(\text{SiO}_2)_x$ , or  $(\text{ZrO}_2)_{1-x}(\text{AlO}_{1.5})_x$  was introduced to the remaining region in the cell in contact with the crystal layer. The thicknesses of the crystal and amorphous layers were 1.7 and 3.4 nm, respectively. The periodic boundary condition was applied in the simulation. The simulations of the annealing were carried out at a constant pressure of 1 atm. The temperature was also kept constant at  $1000^\circ\text{C}$ , which is a typical temperature in the heat process of device fabrication. The program package for the classical molecular dynamic simulation WinMASPHYC<sup>31)</sup> was used. The pair potential by Matsui<sup>32)</sup> was used to describe the interaction between Si, Al, and O. Modified parameters were used for the Si-O interaction. For the pairs containing Zr and/or Hf, potential parameters optimized by Kaneta et al. were used.<sup>30)</sup>

### 3.2 Crystallization and phase separation of aluminate and silicate of Hf and Zr

The results for amorphous Hf-aluminate  $(\text{HfO}_2)_{1-x}(\text{AlO}_{1.5})_x$  with  $x = 0.2$  annealed at  $1000^\circ\text{C}$  are illustrated in **Figure 9**. Figure 9 (a) shows the atomic configuration of the amorphous Hf-aluminate in contact with the crystallized  $\text{HfO}_2$

layer before annealing. O atoms are not shown in the figure. Because the periodic boundary condition is employed in our simulation, crystallized  $\text{HfO}_2$  regions exist on the upper and lower sides of the amorphous Hf-aluminate in Figure 9. The crystallization of the Hf-aluminate proceeds mainly from the regions in contact with the  $\text{HfO}_2$  nucleus. We found that the region with a low Al concentration crystallizes directly, including the Al atoms. On the other hand, in the region with a high Al concentration, the crystallization is accompanied by the diffusion of Al atoms from the crystallizing region to the outside amorphous region. The crystallization is completed after the Al concentration falls below a certain level. The existence of the upper limit of Al concentration in the crystallized region is shown in **Figure 10 (a)**. The Al concentration is lower in the crystallized region and higher in the amorphous region than the average. As a result of the phase separation, crystallization proceeds slower in the remaining amorphous region because of the higher Al concentration. Thus, the crystallization is retarded in the region with a high Al concentration.

We investigated the crystallization rates of Hf-aluminate  $(\text{HfO}_2)_{1-x}(\text{AlO}_{1.5})_x$  in  $1000^\circ\text{C}$  annealing for various Al concentrations. The results are shown in **Figure 11 (a)**. We found that very little suppression is achieved by mixing the Al atoms when  $x$  is less than 0.15. At these concentrations, the Hf-aluminate crystallizes without phase separation. This value corresponds to the above-mentioned upper limit of Al concentration in the crystallized region. On the other hand, when  $x$  is more than 0.2, the crystallization is accompanied by phase separation and takes longer than in the case of low Al concentration.

We also investigated the crystallizations of Hf-silicate  $(\text{HfO}_2)_{1-x}(\text{SiO}_2)_x$  in  $1000^\circ\text{C}$  annealing for various Si concentrations. As in the case of Al, the crystallization of the Hf-silicate occurs directly in lower Si concentrations and is accompanied by a phase separation in higher Si concentrations. The crystallization rates obtained by our simula-

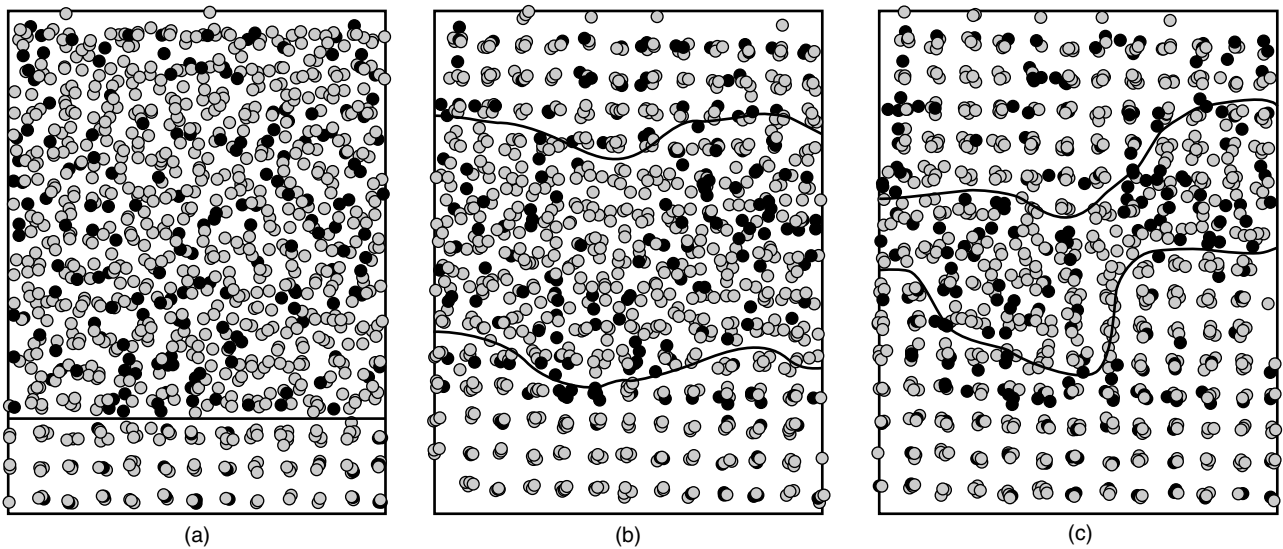


Figure 9 Atomic configuration of  $(\text{HfO}_2)_x(\text{AlO}_{1.5})_{1-x}$  with  $x = 0.2$  after (a) 0 ps (initial configuration), (b) 2000 ps, and (c) 6000 ps annealing at  $1000^\circ\text{C}$ . The shaded circles show Hf atoms. The black ones show Al. The O atoms are not shown in the figure. The bold lines show the boundaries between the crystal and amorphous regions.

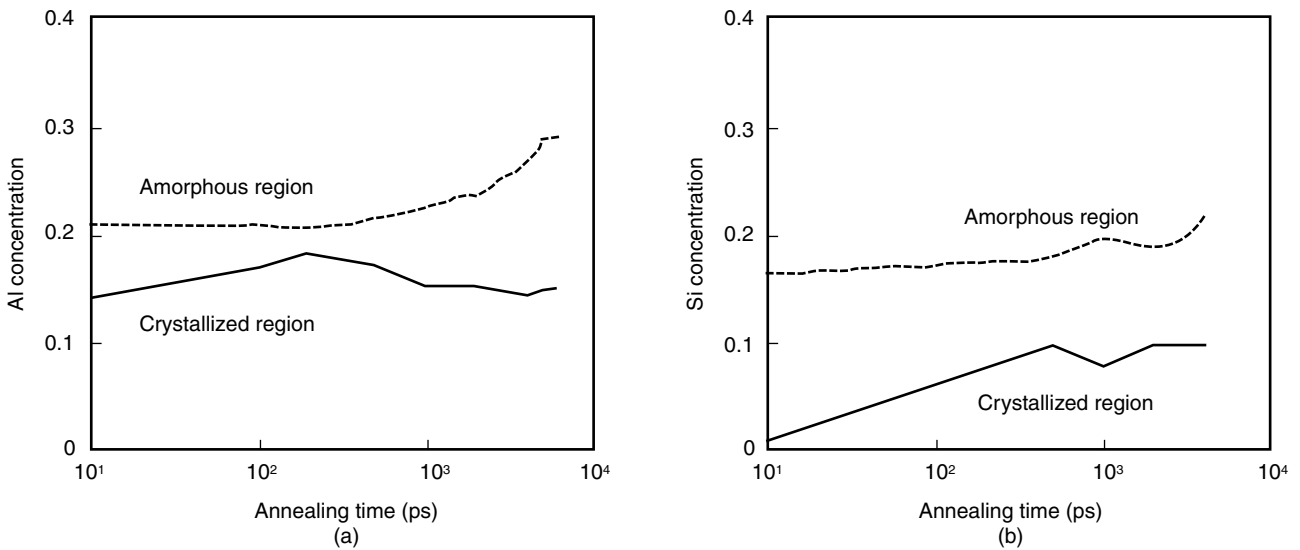


Figure 10 Concentrations of (a) Al in Hf-aluminate  $(\text{HfO}_2)_{1-x}(\text{AlO}_{1.5})_x$  with  $x = 0.2$  and (b) Si in Hf-silicate  $(\text{HfO}_2)_{1-x}(\text{SiO}_2)_x$  with  $x = 0.15$  in amorphous and crystallized regions. The annealing temperature is  $1000^\circ\text{C}$ .

tion for various Si concentrations are shown in **Figure 11 (b)**. Very little suppression of the crystallization is achieved by mixing the Si atoms when  $x$  is less than 0.1. As in the case of Hf-aluminate, this value corresponds to the upper limit of Si concentration in the crystallized region. The

concentrations of Si in the amorphous and crystallized regions are shown in **Figure 10 (b)**. When  $x$  is more than 0.15, the effect on the suppression of the crystallization is larger than in the case of Al.

The crystallizations of the aluminate and the silicate of Zr in  $1000^\circ\text{C}$  annealing were also in-

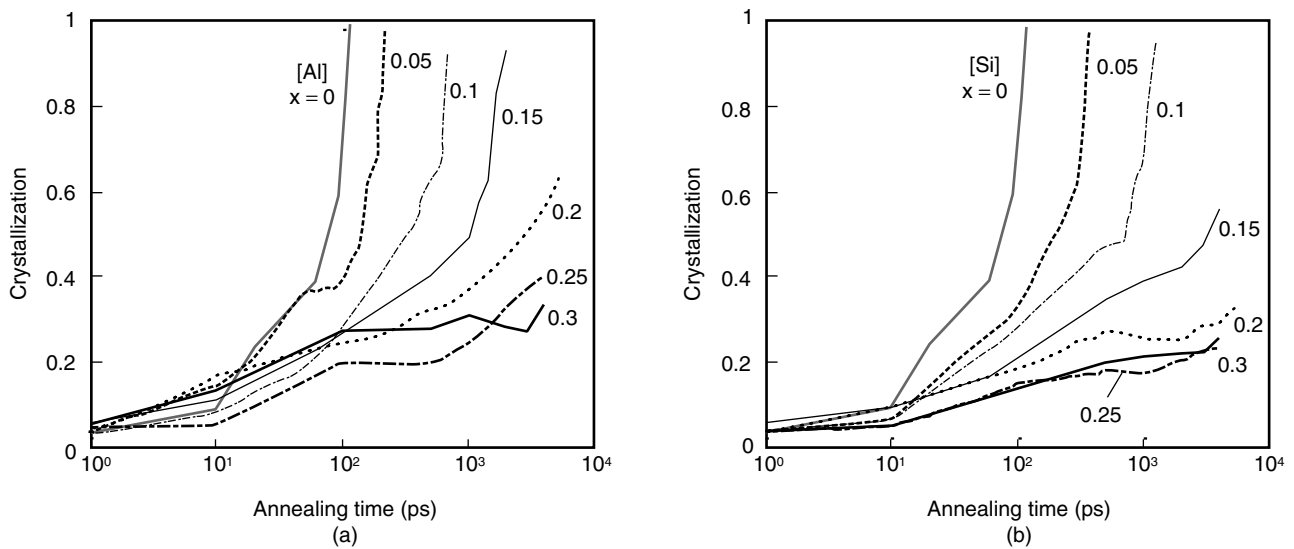


Figure 11 Crystallization of (a) Hf-aluminate  $(\text{HfO}_2)_{1-x}(\text{AlO}_{1.5})_x$  and (b) Hf-silicate  $(\text{HfO}_2)_{1-x}(\text{SiO}_2)_x$  for various compositions. The annealing temperature is  $1000^\circ\text{C}$ .

vestigated. As in the case of Hf-aluminate and Hf-silicate, Si suppresses the crystallization in the alloys of  $\text{ZrO}_2$  more effectively than Al.

#### 4. Conclusions

We investigated the electronic properties of the Si(100)/ $\text{SiO}_2$  interface using the first-principles molecular dynamics method. Based on the results of our calculations, the electronic properties of the interface with and without defects, hydrogen and nitrogen atoms, and the role of the defects and impurities in the trap generation were discussed. We also simulated the crystallization and phase separation of aluminates and silicates of Hf and Zr by employing the classical molecular dynamics method.

From the results of our simulation, we found new phenomena beyond the current model on the Si/ $\text{SiO}_2$  interface and also on the defects and impurities around it. We also understood the mechanism of the crystallization and phase separation of aluminates and silicates of hafnium and zirconium in atomic-scale aspects. The information gives a guide to fabricating high-reliability, advanced gate dielectrics.

#### References

- 1) R. Car and M. Parrinello: Unified Approach for Molecular Dynamics and Density-Functional Theory. *Phys. Rev. Lett.*, **55**, 22, p.2471-2474 (1985).
- 2) P. Hohenberg and W. Kohn: Inhomogeneous Electron Gas. *Phys. Rev.* **136**, 3B, p.B864-B871 (1964).
- 3) D. Vanderbilt: Soft self-consistent pseudopotentials in a generalized eigenvalue formalism. *Phys. Rev.* **41**, 11, p.7892-7895 (1990).
- 4) J. P. Perdew: Electronic Structure of Solids '91 (ed. by P. Ziesche and H. Eschrig), Akademie Verlag, Berlin, 1991.
- 5) A. Ourmazd, D. W. Taylor, and A. Rentschler: Si  $\rightarrow$   $\text{SiO}_2$  transformation: Interfacial structure and mechanism. *Phys. Rev. Lett.*, **59**, 2, p.213-316 (1987).
- 6) T. Shimura, H. Misaki, M. Umeno, I. Takahashi, and J. Harada: X-ray diffraction evidence for the existence of epitaxial microcrystallites in thermally oxidized  $\text{SiO}_2$  thin films on Si(111). *J. Cryst. Growth*, **166**, p.786-791 (1996).
- 7) V. V. Afanas'ev and A. Stesmans: Epitaxial Growth of  $\text{SiO}_2$  Produced in Silicon by Oxygen

- Ion Implantation. *Phys. Rev. Lett.*, **77**, 20, p.4206-4209 (1996).
- 8) N. Awaji, Y. Sugita, T. Nakanishi, S. Okubo, K. Takasaki, and S. Komiya: High-precision x-ray reflectivity study of ultrathin SiO<sub>2</sub> on Si. *Journal of Vacuum Science & Technology A: Vacuum, Surfaces, and Films. J. Vac. Sci. Technol. A14*, **14**, 3, p.971-976 (1996).
  - 9) C. Kaneta, T. Yamasaki, T. Uchiyama, T. Uda, and K. Terakura: Structure and electronic property of Si(100)/SiO<sub>2</sub> interface. *Microelectronic Engineering* **48**, p.117-120 (1999).
  - 10) T. Yamasaki, C. Kaneta, T. Uchiyama, T. Uda, and K. Terakura: Geometric and electronic structures of SiO<sub>2</sub>/Si(001) interfaces. *Phys. Rev. B*, **63**, 11, p.115314-115318 (2001).
  - 11) D. A. Muller, T. Sorsch, S. Moccio, F. H. Baumann, K. Evans-Lutterodt, and G. Timp: The electronic structure at the atomic scale of ultrathin gate oxides. *Nature*, **399**, p.758-761 (1999).
  - 12) E. H. Poindexter, P. J. Caplan, B. E. Deal, and R. R. Razouk: Interface states and electron spin resonance centers in thermally oxidized (111) and (100) silicon wafer. *J. Appl. Phys.*, **52**, 2, p.879-884 (1981).
  - 13) J. L. Cantin, M. Schoisswohl, H. J. von Bardeleben, N. H. Zoubir, and M. Vergnat: Electron-paramagnetic-resonance study of the microscopic structure of the Si(001)-SiO<sub>2</sub> interface. *Phys. Rev. B*, **52**, 16, p.R11599-R11602 (1995).
  - 14) G. J. Gerardi, E. H. Poindexter, P. J. Caplan, and N. M. Johnson: Interface traps and P<sub>b</sub> centers in oxidized (100) silicon wafers. *Appl. Phys. Lett.*, **49**, 6, p.348-350 (1986).
  - 15) A. Aubert, H. J. von Bardelben, F. Delmotte, J. L. Cantin, and M. C. Hugon: Electron-paramagnetic-resonance study of the (100)Si/Si<sub>3</sub>N<sub>4</sub> interface. *Phys. Rev. B*, **59**, 16, p.10677-10684 (1999).
  - 16) A. Stesmans, B. Nowen, and V. V. Afanas'ev: P<sub>bi</sub> interface defect in thermal (100)Si/SiO<sub>2</sub>: <sup>29</sup>Si hyperfine interaction. *Phys. Rev. B*, **58**, 23, p.15801-15809 (1998).
  - 17) C. Kaneta, T. Yamasaki, T. Uchiyama, T. Uda, and K. Terakura: DEFECT STATES DUE TO SILICON DANGLING BONDS AT THE Si(100)/SiO<sub>2</sub> INTERFACE AND THE PASSIVATION BY HYDROGEN ATOMS. *Mat. Res. Soc. Symp. Proc.*, Vol.592, Boston, 2000, Materials Research Society, p.39-44.
  - 18) A. H. Edwards: THEORY OF DEFECTS IN THE MOS SYSTEM. *The Physics and Chemistry of SiO<sub>2</sub> and the SiO<sub>2</sub> interface*, edited by C. R. Herms and B. E. Deal, Georgia, 1988, Electrochemical Society, Plenum, New York, 1988, p.271-283.
  - 19) M. Sakashita, S. Zaima, Y. Koide, and Y. Yasuda: Observation of Si-SiO<sub>2</sub> interface states within the conduction band by tunneling current spectroscopy. *Appl. Surf. Sci.* **56-58**, p.841-845 (1992).
  - 20) B. Tuttle and C. G. Van de Walle: Structure, energetics, and vibrational properties of Si-H bond dissociation in silicon. *Phys. Rev. B*, **59**, 20, p.12884-12889 (1999).
  - 21) C. G. Van de Walle and R. A. Street: Structure, energetics, and dissociation of Si-H bonds at dangling bonds in silicon. *Phys. Rev. B*, **49**, 20, p.14766-14769 (1994).
  - 22) Ph. Avouris, R. E. Walkup, A. R. Rossi, H. C. Akpati, P. Nordlander, T. -C. Shen, G. C. Abeln, and J. W. Lyding: Breaking individual chemical bonds via STM-induced excitations. *Surf. Sci.* **363**, p.368-377 (1996).
  - 23) C. Kaneta, T. Yamasaki, and T. Uda: Reaction of atomic hydrogen with the Si(100)/SiO<sub>2</sub> interface defects. *Proc. 25th Int. Conf. on the Physics of Semiconductors (Proceedings in Physics, Springer Vol.87)*, edited by N. Miura and T. Ando, Osaka, 2000, p.419-420.
  - 24) K. L. Brower: Dissociation kinetics of hydrogen-passivated (111) Si-SiO<sub>2</sub> interface defects. *Phys. Rev. B*, **42**, 6, p.3444-3453 (1990).
  - 25) R. I. Hegde, B. Maiti, and P. J. Tobin: Growth

- and Film Characteristics of N<sub>2</sub>O and NO Oxynitride Gate and Tunnel Dielectrics. *J. Electrochem. Soc.* **144**, 3, p.1081-1086 (1997).
- 26) N. Kimizuka, K. Yamaguchi, K. Imai, T. Iizuka, C. T. Liu, R. C. Keller, and T. Horiuchi: NBTI enhancement by nitrogen incorporation into ultrathin gate oxide for 0.10- $\mu$ m gate CMOS generation. Symp. on VLSI Technol. Digest of Technical Papers, Honolulu, 2000, p.92-93.
- 27) T. Yamasaki and C. Kaneta: Mechanisms of Nitrogen Segregation and Hole Trap Generation at the Interface of SiO<sub>2</sub>/Si(001). Extended Abs. of the 2002 Int. Conf. on Solid State Devices and Materials, Nagoya, 2002, p.750-751.
- 28) H. Heyns, H. Bender, R. Cartier, M. Caymax, T. Conard, S. De Gendt, R. Degraeve, H. De Witte, G. Groeseneken, S. Haukka, K. Henson, M. Houssa, S. Kubicek, J. W. Maes, N. Naili, H. Nohira, W. Tsai, M. Tuominen, W. Vandervorst, R. Wilhelm, E. Young, and C. Zhao: High-k dielectric materials prepared by Atomic Layer CVD. Conference Proceedings of "Insulating Films on Semiconductors 2001," p.99.
- 29) Y. Morisaki, Y. Sugita, K. Irino, and T. Aoyama: Effects of Interface Oxide Layer on HfO<sub>2</sub> Gate Dielectrics. Conference Proceedings of "International Workshop on Gate Insulator (IWGI) 2001," Tokyo, 2001.
- 30) C. Kaneta, Y. Kosaka, and T. Yamasaki: Molecular Dynamic Simulation on the Crystallization of High-k Gate Dielectric Materials. To be published in Proc. of International Semiconductor Technology Conference, Tokyo, 2002.
- 31) WinMASPHYC 2.0 Ultra (Fujitsu, 2001). <http://software.fujitsu.com/jp/winmasphyc/>
- 32) M. Matsui: Molecular dynamics study of the structures and bulk moduli of crystals in the system CaO-MgO-Al<sub>2</sub>O<sub>3</sub>-SiO<sub>2</sub>. *Phys. Chem. Materials*, **23**, p.345-353 (1996).



**Chioko Kaneta** received the B.S., M.S., and D.S. degrees in Physics from Tohoku University, Sendai, Japan in 1980, 1982, and 1985, respectively. She joined Fujitsu Laboratories Ltd., Kawasaki, Japan in 1985, where she has been engaged in research of Si crystals, gate dielectrics, and the interfaces between them for advanced silicon devices. She is a member of the Japan Society of Applied Physics and the Physical Society of Japan.



**Yuko Kosaka** received the B.S. and M.S. degrees in Applied Physics from the University of Tokyo, Tokyo, Japan in 1999 and 2001, respectively. She joined Fujitsu Laboratories Ltd., Atsugi, Japan in 2001, where she has been engaged in research and development of advanced CMOS devices. She is a member of the Japan Society of Applied Physics.



**Takahiro Yamasaki** received the B.S. degree from Kyoto University, Kyoto, Japan in 1984 and the Dr. Eng. degree in Solid State Physics from Osaka University, Osaka, Japan in 1989. He joined Fujitsu Laboratories Ltd., Atsugi, Japan in 1989, where he has been engaged in research of semiconductor devices using computer simulations. He is a member of the Physical Society of Japan and the American Physical Society.